Harmonic Resonance Analysis and Suppression for Suburban Railway Continuous Power Supply Systems

Fan Zhong, Shaofeng Xie, You Peng, and Xinyao Hu

***Abstract*—The continuous power supply system, which eliminates the neutral section and realizes safe and reliable operation, shows a development trend in suburban railways. However, the access of a power quality compensator (PQC) may alter the impedance characteristics of the system and introduce additional harmonics with a broader frequency band, potentially increasing the risk of resonance. Accordingly, in this paper, an analytical method is first adopted in conjunction with a field test to construct a simplified harmonic model for an actual continuous suburban line. A modal scanning algorithm is then used to analyze the effects of the controller and filter in the PQC on the harmonic resonance of the suburban railway continuous power supply system. Based on the improved particle swarm optimization algorithm, a multi-objective optimization design for PQC is proposed that can suppress harmonic resonance, filter the harmonics, and reduce the cost while preserving the stability of the control system. Finally, a real case study based on the field test demonstrates the effectiveness of the proposed design.**

***Index Terms*—Suburban railway, continuous power supply system, resonance characteristic, modal scan algorithm, multi-objective optimization design, field test.**

I. Introduction

With the expansion of metropolitan areas, suburban railways will develop into continuous networks with faster speed and increasing passenger flow. To achieve safe, timely, and reliable suburban railway services, the power supply system will gradually transform from the existing unilateral power supply mode into a continuous power supply mode [1], [2]. In contrast to the existing unilateral power supply mode, the continuous power supply mode has the following advantages: ① the neutral section can be eliminated to ensure the continuity of power supply; ② the voltage loss caused by the traction network can be reduced and the power supply capacity can be enhanced by simultaneous power supplies from multiple traction substations (TSs) to trains [3]-[6]; ③ the power quality compensator (PQC) can solve power quality problems such as negative sequence and reactive power [7]-[9].

Harmonic resonance is currently attracting considerable attention because of the potential risks associated with the safe operation of suburban railways. Although for decades, resonance accidents have taken place in suburban railways with unilateral power supply modes, they remain an unresolved issue [10]. The resonance characteristics of suburban railways become more complicated once the TS is outfitted with a PQC to realize a continuous power supply. In addition, the factors affecting the resonance differ significantly from those observed in the unilateral power supply mode [11]. At the same time, the PQC and various types of electric locomotives collectively form a harmonic source, which suggests that a broader spectrum of harmonics is present in the suburban railway continuous power supply system (SRCPSS). The coincidence of the resonance point and harmonic source in frequency results in abnormal electrical phenomena such as resonance overvoltage and overcurrent [12], [13].

Many studies have investigated the resonance issues of power systems and suburban railways. In contrast to power systems, resonance accidents that occur in suburban railways are typically characterized by parallel resonance due to the large leakage inductor of the onboard transformers in electric locomotives [14], [15]. Studies on parallel resonance are divided into three main steps. The first step is to establish a harmonic model of the SRCPSS. The modeling of traction networks, transformers, and electric locomotives has been relatively mature [16], [17]. However, simulation and computational models of locomotives generally differ from field test data at low frequencies to some extent. In addition, the research on harmonic modeling of PQCs remains in its infancy. Further investigation is therefore required to quantify the differences between PQCs and electric locomotives and to model SRCPSSs using field tests and theoretical calculations.

Resonance analysis is the second step in solving the resonance issue. The analytical methods for parallel resonance characteristics can be summarized into three types: simulation analysis, frequency scanning, and modal analysis [18]. Simulation analysis is relatively efficient, which can obtain the impedance-frequency characteristics and reflect the relationship between the impedance and voltage at each frequen-

Manuscript received: March 31, 2024; revised: July 7, 2024; accepted: July 28, 2024. Date of CrossCheck: July 28, 2024. Date of online publication: August 20, 2024.

This work was supported in part by the National Natural Science Foundation of China (No. 52277126).

F. Zhong, S. Xie (corresponding author), Y. Peng, and X. Hu are with the School of Electrical Engineering, Southwest Jiaotong University, Chengdu 611756, China (e-mail: zf020131416@163. com; sfxie@swjtu. edu. cn; pengyou@my.swjtu.edu.cn; xinyaohuhxy@163.com).

DOI: 10.35833/MPCE.2024.000348

cy. Nevertheless, the models in the simulation software are typically fixed and idealized, resulting in discrepancies between the impedance frequency characteristics of the simulated power system and those of the actual power system. The frequency scanning method can accurately obtain the resonance characteristics, but does not provide additional information that can be used to suppress the resonance. The modal analysis method is more comprehensive, but the calculation process is complex [19] - [21]. Consequently, for a SRCPSS with more complex influencing factors and topologies, a more efficient and accurate method is required for obtaining resonance characteristics.

The third step is to suppress the resonance. Installing filters in the TS or adjusting the pulse width modulation (PWM) strategy of locomotives is common method for resonance suppression. Carrier-phase-shifted PWM (CPS-PWM) can increase the equivalent switching frequency to reduce low-frequency (LF) harmonics, but it cannot completely eliminate the current harmonics that tend to cause resonance. A windowed selective harmonic elimination PWM method for controlling locomotives is introduced in [22], which can control the harmonic resonance to some extent, but is difficult to realize. An active power filter can dynamically and accurately compensate for LF harmonics but cannot resolve high-frequency (HF) resonance [23]. The most effective method for resolving resonance issues involves using different passive filters. This method enables the filtration of harmonics and alteration of the resonance point. However, it has the disadvantages of high cost and power loss [24]. The inclusion of a PQC can significantly alter the impedance characteristics of suburban railways to a large extent. Therefore, prevention at the design stage of an SRCPSS is the simplest and most cost-effective means of suppressing resonance.

As the proportion of power electronic equipment in power systems gradually increases, many studies have proposed different designs for control strategies and filters of PQCs [25]. The design of control strategy is chiefly concerned with stability. Many studies have proposed the addition of active damping to the control link to enhance the steady-state performance of the power system. These studies have also investigated the effects of different active damping methods on stability [26]-[29]. However, the effects of the filters on the design of the control strategy have not been considered. Filters mainly include the L, LC, LCL, and LLCL types [30], [31]. Due to its advantages of excellent attenuation of HF harmonics, low investment costs, and multiple selective control modes, the LCL filters is extensively used in converters. The design of LCL filters focuses on ripple current, HF harmonics, reactive power, and LCL resonance peaks while ignoring the effects of control parameters on the filtering effect [32], [33]. In summary, the current designs for the control and filtering parameters are independent, and the interaction between them is not considered. Simultaneously, the control and filtering parameters in power electronic equipment such as PQCs affect the impedance characteristics of the power system, which means that a reasonable design of the control and filtering parameters can attenuate the resonance to a certain extent [34], [35]. Therefore, studies must be focused on evaluating the effects of PQCs on resonance and preventing resonance through proper PQC design.

To address the aforementioned resonance issues, this paper investigates the complete resonance characteristics of an SRCPSS under multi-locomotive operating conditions and solves the resonance issues in suburban railways by changing the resonance characteristics of the PQC.

The main contributions of this paper are described as follows.

1) An analytical method and field test are combined to establish a simplified harmonic model for the PQC and electric locomotive. An HF-dominated impedance model of the PQC and locomotive is built according to the control strategy to provide an admittance matrix for modal scanning.

2) Based on modal analysis, a modal scanning algorithm is used to reveal the resonance characteristics of the SRCPSS. A multi-objective optimization design for the PQC is then proposed, which achieves resonance suppression, harmonic filtering, and cost reduction while preserving the stability of the control system.

3) Using an actual suburban line as a case, the resonance characteristics are shown through field test and simulation, and the effect of the proposed optimization design is evaluated using the resonance suppression efficiency (RSE) indicator.

II. Harmonic Equivalent Model of an SRCPSS

A. Structure of an SRCPSS

Figure 1 shows the typical topology of an SRCPSS. The high-voltage side of the TS is connected to a 110 kV busbar with a short-circuit capacity of 1000 MVA. The mixed connection mode of n back-to-back converters is adopted by the PQC. The β-side of each converter is connected in cascade to the balanced connection transformer (BCT) through the L filter, and the α-side of each converter is connected to the LCL filter after a parallel structure is formed via the step-up transformer. The high-voltage winding of the step-up transformer is connected to a 27.5 kV traction network.

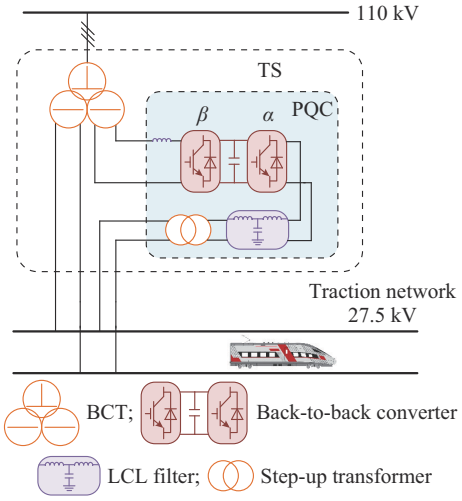

Fig. 1. Typical topology of an SRCPSS.

B. Transformer Model

The BCT shown in Fig. 1 is composed of two single-

phase transformers (T1 and T2). Figure 2 shows the specific structure of BCT. Here, the primary winding of T1 is connected to the 110 kV busbar (A and B phases), and the primary winding of T2 is connected to the midpoint of the primary winding of T1 and the C-phase busbar. The β-phase differs from the α-phase by 90°.

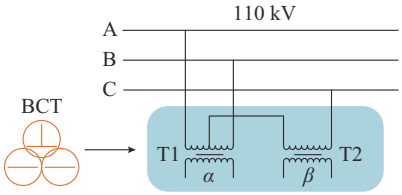

Fig. 2. Specific structure of BCT.

The single-phase transformer is used as an example for modeling because the transformers in the SRCPSS are all combined from single-phase transformers. The equivalent circuit of the transformer consists of R_1, X_T, and R_2, where R_1 is the ohmic loss, and the harmonic inductance is represented by the parallel connection of X_T and R_2, X_T is the leakage inductance at the fundamental frequency, and R_2 is the harmonic resistance. The impedance angle θ is defined by the transformer capacity [16].

R_1, R_2, and θ are expressed as:

$$\begin{cases} R_1 = X_T/\tan\theta \\ R_2 = 10X_T\tan\theta \\ \tan\theta = e^{0.693+0.769\ln S_T - 0.042(\ln S_T)^2} \end{cases} \tag{1}$$

where S_T is the rated capacity of the transformer.

The complete expression for the transformer impedance is:

$$Z_T = R_1 + (R_2 // jhX_T) = \frac{X_T}{\tan\theta} + \frac{\dfrac{h^2 X_T}{10\tan\theta} + jhX_T}{1+\left(\dfrac{h}{10\tan\theta}\right)^2} \tag{2}$$

where h is the harmonic order. Here, $h^2X_T/(10\tan\theta)$ is used to describe the eddy current loss, and $1/\{1+[h/(10\tan\theta)]^2\}$ is used to describe the demagnetization effect because it reduces the leakage inductance of the transformer to a certain extent.

The equivalent impedances Z_α and Z_β of the low-voltage side of T1 and T2 can be obtained by combining the power system impedance and the transformer impedance of the BCT. The specific equations are given as:

$$\begin{cases} Z_\alpha = 2Z_S/K_{T1}^2 + Z_{T1} \\ Z_\beta = 3Z_S/2K_{T2}^2 + Z_{T2} \end{cases} \tag{3}$$

where Z_S is the harmonic impedance of the power system; K_{T1} and K_{T2} are the voltage transformation ratios of T1 and T2, respectively; and Z_{T1} and Z_{T2} are the harmonic equivalent impedances of T1 and T2, respectively.

C. PQC Model

The structure of a typical PQC is composed of an L filter, n back-to-back converters, n LCL filters, and a step-up transformer, as shown in Fig. 3. Note that the studied model in this paper is shown in black lines and symbols, while the gray parts are ignored in this paper. Each of the n low-voltage windings of the step-up transformer is connected to n back-to-back converters. The back-to-back converter consists of α- and β-phase converters. The modulation signal reconstruction method is adopted by the β-phase converters to realize the balanced control of the direct current (DC) voltage, and CPS-PWM is used in the α- and β-phase converters. As the effects of DC-side voltage control on HF harmonic resonance can be negligible [36], the sole requirement is to establish the impedance model of the PQC through the control strategy of α-phase converters. The current loop of α-phase converters is realized by sampling the current signals i_1-i_n and the voltage signals u_{m1}-u_{mn}. Current signals i_{C1}-i_{Cn} flowing through the capacitors are also sampled for active damping.

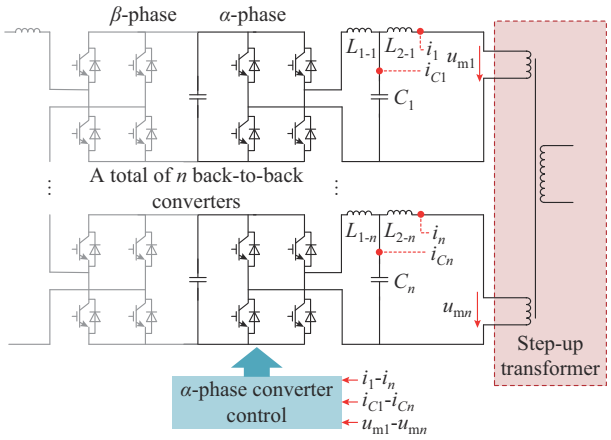

Fig. 3. Structure of a typical PQC.

Take the k^{th} α-phase converter as an example for analysis. Figure 4(a) shows the control with feedback lines in red color. Note that the i_k closed-loop and i_{Ck} feedback controls are adopted from [11] to achieve accurate tracking of the reference current i_{kref}, where i_k and i_{Ck} are the currents of the branch where the inductor $L_{2\text{-}k}$ and capacitor C_k are located, respectively. A proportional resonance (PR) current controller is used, and the transfer function $G_{PR}(s)$ is given in (4). To realize accurate modeling of the converter, the transfer function $G_d(s)$ in (5), which reflects the delay of the digital control, is introduced into the control strategy, and $G_d(s)$ is approximately 1.5 times larger than the sampling period. K_C is the coefficient of active damping; and K_{PWM} is the ratio of the DC-side voltage to the triangular carrier voltage. Finally, the k^{th} α-phase converter in Fig. 3 can be equivalent to the Thevenin circuit presented, as shown in Fig. 4(b).

$$G_{PR}(s) = K_p + \frac{K_r\omega_{co}s}{s^2 + 2\omega_{co}s + \omega_r^2} \tag{4}$$

$$G_d(s) = e^{-1.5T_d s} \approx \frac{1 - 1.5T_d s/2 + (1.5T_d s/12)^2}{1 + 1.5T_d s/2 + (1.5T_d s/12)^2} \tag{5}$$

where K_p is the proportion control coefficient; K_r is the resonance control coefficient; ω_{co} is the cut-off angular frequency of the PR controller; ω_r is the fundamental angular frequency; and T_d is the sampling period. Equation (4) shows that the change in K_r has little effect on G_{PR}. Therefore, the effect of K_r on the resonance of the SRCPSS is not considered.

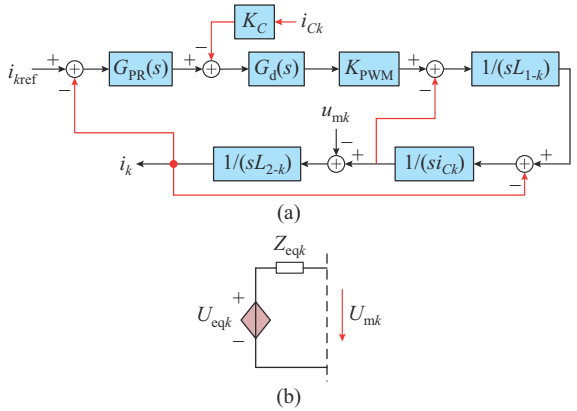

Fig. 4. Harmonic equivalent model of the k^{th} α-phase converter. (a) Control diagram. (b) Thevenin equivalent circuit.

According to Thevenin's theorem and the modulation characteristics of converters, the equivalent voltage U_{eqk} and equivalent impedance Z_{eqk} can be obtained as [11], [21], [37]:

$$\begin{cases} U_{eqk}(s)=G_{PR}(s)G_d(s)K_{PWM}i_{kref}/(1+sC_kK_CG_d(s)K_{PWM}+ \\ \qquad s^2L_{1\text{-}k}C_k)+u_{hk} \\ Z_{eqk}(s)=[s(L_{1\text{-}k}+L_{2\text{-}k})+G_d(s)K_{PWM}(G_{PR}(s)s^2L_{2\text{-}k}C_kK_C)+ \\ \qquad s^3L_{1\text{-}k}L_{2\text{-}k}C_k]/(1+sC_kK_CG_d(s)K_{PWM}+s^2L_{1\text{-}k}C_k) \end{cases} \tag{6}$$

where the subscript k denotes the k^{th} α-phase converter; and u_{hk} is the harmonic component generated by the k^{th} α-phase converter due to modulation.

As (7) shows, u_{hk} primarily consists of two parts: the HF harmonic components u_{HFk} associated with the switching frequency, and the LF harmonic components u_{LFk} derived from the field test [17], [33], [38].

$$\begin{cases} u_{hk}=u_{HFk}+u_{LFk} \\ u_{HFk}=\sum_{m=2,4,6,\dots}\sum_{n=\pm1,\pm3,\pm5,\dots}4u_{dc}(-1)^{m/2}/(m\pi)\cdot \\ \qquad J_n(m\pi M_r/2)\sin(m\omega_c t+n\omega_0 t) \\ J_n(x)=\sum_{b=0}^{\infty}\frac{(-1)^k}{b!(b+n)!}(x/2)^{2b+n} \end{cases} \tag{7}$$

where u_{dc} is the DC-side voltage; J_n is the Bessel function of the first type; M_r is the modulation depth; ω_c is the angular frequency of the carrier signal; and ω_0 is the angular frequency of the modulation signal.

The equivalent voltage u_{PQC} and equivalent impedance Z_{PQC} of the PQC can be obtained from (8) by combining and simplifying the corresponding models of n back-to-back converters and the step-up transformer.

$$\begin{cases} u_{PQC}=u_{eqk}K_{ST} \\ Z_{PQC}=Z_{eqk}K_{ST}^2/n+Z_{ST} \end{cases} \tag{8}$$

where K_{ST} is the transformation ratio of the high-voltage winding to the low-voltage winding of the step-up transformer; and Z_{ST} is the harmonic equivalent impedance of the step-up transformer.

As (6) and (8) show, the value of Z_{eqk} increases considerably after multiplying with K_{ST}, and Z_{eqk} mainly consists of parameters $L_{1\text{-}k}$, $L_{2\text{-}k}$, C_k, K_p, and K_C, which significantly affect the resonance.

D. SRCPSS Model

Figure 5 shows the complete SRCPSS model, where the blue box represents the harmonic equivalent model of the TS. With TS1 used as an example, U_{PQC1} is the equivalent voltage source of the high-voltage winding of the step-up transformer; Z_{PQC1} is the harmonic equivalent impedance of the PQC and the step-up transformer; U_{S1} is the equivalent voltage source of the low-voltage winding of T1; and $Z_{\alpha1}$ is the equivalent harmonic impedance of the power system and T1. The purple and yellow boxes represent the equivalent π-circuit of the traction network and the electric locomotive model, respectively. The specific models of the traction network and locomotive are presented in Supplementary Material A. The SRCPSS model is a dynamic model in which an electric locomotive moves along a traction network.

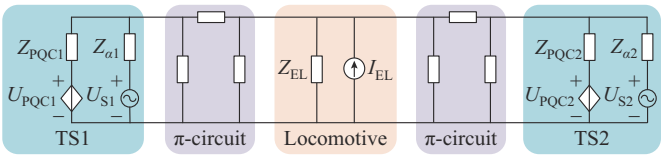

Fig. 5. Complete SRCPSS model.

Figure 5 shows that when the continuous power supply mode is adopted, the TS model changes, and the traction network simultaneously becomes longer, resulting in a major shift in the structure of the suburban railway. The equivalent impedances $Z_{C\text{-}TS1}$ and $Z_{U\text{-}TS1}$ of the TS in the continuous and unilateral power supply modes are given in (9). In general, the large value of Z_S, $Z_{U\text{-}TS1}$ is approximately several times larger than $Z_{C\text{-}TS1}$, which leads to a large increase in the resonance frequency, and $L_{1\text{-}k}$, $L_{2\text{-}k}$, C_k, K_p, and K_C in the PQC significantly affect $Z_{C\text{-}TS1}$. Therefore, altering the aforementioned parameters can successfully regulate the resonance to ensure the stability of the control system.

$$\begin{cases} Z_{C\text{-}TS1}=\dfrac{Z_{PQC1}Z_{\alpha1}}{Z_{\alpha1}+Z_{PQC1}} \\ Z_{U\text{-}TS1}=Z_{\alpha1}=2Z_S/K_{T1}^2+Z_{T1} \end{cases} \tag{9}$$

III. Resonance Characteristics of SRCPSS and Multi-objective Optimization Design for PQC

The basic idea of modal analysis is that parallel resonance occurs only when the admittance matrix of the system approaches a singularity. Therefore, the eigenvalues of the matrix contain resonance information, and the main purpose of modal analysis is to find resonance peaks using eigenvalues [21].

A. Resonance Characteristics of SRCPSS

Based on the modal analysis, a modal scanning algorithm is adopted to scan eigenvalues at different parameters and frequencies to derive the resonance characteristics. The specific process is illustrated in Fig. 6, where v_1 and v_2 are the ranges of the resonance influencing factors; h_1 and h_2 are the

ranges of the harmonic order; and Δv and Δh are the step sizes of v and h, respectively.

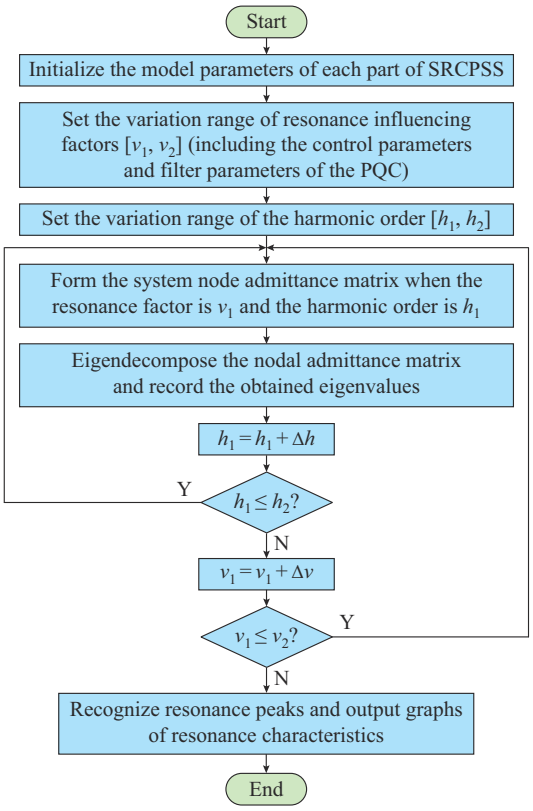

Fig. 6. Flow chart of modal scanning algorithm.

B. Resonance Prevention of SRCPSS

The use of passive filters requires additional space in the TS and increases the investment cost. The previous analysis shows that the PQC significantly affects the resonance frequency and impedance amplitude of the SRCPSS. Therefore, this paper proposes a multi-objective optimization design based on an improved particle swarm optimization algorithm to enable the PQC to prevent resonance.

First, the ranges of $L_{1\text{-}k}$, $L_{2\text{-}k}$, and C_k must be determined based on the power factor and filtering requirements. The first step is to determine the upper limits of $L_{1\text{-}k}$ and $L_{2\text{-}k}$. The filtering effect is positively related to the total value of the inductors. However, as this value increases, the power factor decreases, which results in problems such as increased device volume and cost. Therefore, the maximum value $L_{Tk,\max}$ of the two inductors in the LCL filter can be obtained as [33]:

$$L_{Tk,\max} = \frac{\sqrt{u_{dck}^2 - u_{mk,\text{peak}}^2}}{2\pi f_0 i_{k,\text{peak}}} \tag{10}$$

where u_{dck} is the DC voltage of the k^{th} back-to-back converter; $u_{mk,\text{peak}}$ is the peak of u_{mk}; $i_{k,\text{peak}}$ is the peak of i_k; and f_0 is the fundamental frequency of the alternating current (AC) system.

In actual projects, the ripple current flowing through the inductors must be less than 20% of $i_{k,\text{peak}}$. Therefore, the lower limit of the two inductors is:

$$L_{Tk,\min} = \frac{(u_{dc} - u_{mk})u_{mk}}{f_{sw}(20\% \cdot i_{k,\text{peak}})u_{dc}} \tag{11}$$

where f_{sw} is the switching frequency.

For capacitor C_k, the reactive power generated by C_k generally must not exceed 5% of the active power of the α-phase converter. Therefore, the maximum value $C_{k,\max}$ is:

$$C_{k,\max} = \frac{5\% \cdot P_\alpha}{2\pi f_0 u_{mk}^2} \tag{12}$$

where P_α is the active power generated by the α-phase converter.

The next step is to determine the values of K_p and K_C based on the stability requirements of the control system. The transfer function of the control system is given by the following equation. As an increase in the LCL filter parameters affects the stability of the control system, the effects of K_p and K_C on the poles of the control system are explored in the context of setting C_k and the total value of inductors L_{Tk} to their maximum values.

$$\begin{cases} G(s) = \dfrac{s^2 A_7 + sA_8 + A_9}{s^5 A_1 + s^4 A_2 + s^3 A_3 + s^2 A_4 + sA_5 + A_6} \\ A_1 = L_{1\text{-}k} L_{2\text{-}k} C_k \\ A_2 = (2\omega_{co} L_{1\text{-}k} + K_C G_d(s) K_{PWM}) L_{2\text{-}k} C_k \\ A_3 = L_{1\text{-}k} L_{2\text{-}k} C_k \omega_0^2 + 2K_C \omega_{co} L_{2\text{-}k} C_k G_d(s) K_{PWM} + L_{1\text{-}k} + L_{2\text{-}k} \\ A_4 = (K_p + 2\omega_{co} L_{2\text{-}k}) G_d(s) K_{PWM} + 2\omega_{co}(L_{1\text{-}k} + L_{2\text{-}k}) + \\ \qquad K_C \omega_0^2 L_{2\text{-}k} C_k G_d(s) K_{PWM} \\ A_5 = (2\omega_{co} K_p + K_r \omega_{co}) G_d(s) K_{PWM} + \omega_0^2 (L_{1\text{-}k} + L_{2\text{-}k}) \\ A_6 = K_p \omega_0^2 G_d(s) K_{PWM} \\ A_7 = K_p G_d(s) K_{PWM} \\ A_8 = (K_r + 2K_p) \omega_{co} G_d(s) K_{PWM} \\ A_9 = K_p \omega_0^2 G_d(s) K_{PWM} \\ p = \text{roots}(G(s)) \\ \max(\text{real}(p(1), p(2), p(3), p(4), p(5))) < 0 \end{cases} \tag{13}$$

where p represents the five poles of the control system; and roots(·) is the root-finding function.

The third step is to determine the optimization goals. Due to modulation, the PQC mainly generates LF and HF harmonics related to the switching frequency. As the PQC can filter out LF harmonics, it is necessary to evaluate the attenuation capability of HF harmonics using the LCL filter to avoid the occurrence of HF resonance in the SRCPSS. According to (7), the frequencies of the voltage harmonics are $(m\omega_c/\omega_0 + n)$ harmonic orders. When the corresponding angular frequency is set to be ω_{mn}, the HF harmonic distortion rate D_{HF} of the AC-side current passing through the LCL filter can be obtained by:

$$D_{HF} = \sum_{m=2,4,6,\ldots} \sum_{n=\pm1,\pm3,\pm5,\ldots} \frac{\left|u_{HFk}(\omega_{mn})\right| \cdot 100\%}{i_{k,\text{peak}} \left|(L_{1\text{-}k} + L_{2\text{-}k})\omega_{mn} - L_{1\text{-}k} L_{2\text{-}k} C_k \omega_{mn}^3\right|} \tag{14}$$

The optimization goal I (OG I) is set to limit the HF harmonics to be 0.3% according to the requirements of IEEE Standard 519-2022. The fitness value of OG I is F_1.

$$\text{OG I: } D_{\text{HF}} \le 0.3\% \tag{15}$$

The OG II is to ensure a better filtering effect and to reduce the investment cost and size of LCL filter. To achieve these, the inductors $L_{1\text{-}k}$ and $L_{2\text{-}k}$ must satisfy the conditions in (16). The fitness value of OG II is F_2.

$$\text{OG II: } \begin{cases} L_{Tk,\min} \le L_{1\text{-}k} + L_{2\text{-}k} \le L_{Tk,\max} \\ L_{1\text{-}k} > L_{2\text{-}k} \end{cases} \tag{16}$$

The OG III is based on the resonance distribution obtained by the modal scanning algorithm and the harmonic band (HB) generated by the PQC and electric locomotives obtained from field test. Resonance can be prevented by shifting or suppressing the resonance band (RB) corresponding to the HB. The fitness value for OG III is F_3.

$$\begin{cases} \boldsymbol{U} = \boldsymbol{Y}^{-1}\boldsymbol{I} \Rightarrow \boldsymbol{Y} = \boldsymbol{L}\boldsymbol{\Lambda}\boldsymbol{T} \Rightarrow \boldsymbol{L} = \boldsymbol{T}^{-1} \Rightarrow \boldsymbol{T}\boldsymbol{U} = \boldsymbol{\Lambda}^{-1}\boldsymbol{T}\boldsymbol{I} \\ \boldsymbol{V} = \boldsymbol{T}\boldsymbol{U} \\ \boldsymbol{J} = \boldsymbol{T}\boldsymbol{I} \\ \begin{bmatrix} V_1 \\ V_2 \\ \vdots \\ V_n \end{bmatrix} = \begin{bmatrix} \lambda_1^{-1} & 0 & \cdots & 0 \\ 0 & \lambda_2^{-1} & \cdots & 0 \\ \vdots & \vdots & & \vdots \\ 0 & 0 & \cdots & \lambda_n^{-1} \end{bmatrix} \begin{bmatrix} J_1 \\ J_2 \\ \vdots \\ J_n \end{bmatrix} \\ \text{OG III: } \max\left| \lambda_1^{-1}, \lambda_2^{-1}, ..., \lambda_n^{-1} \right|_{\text{HB}} \le \varepsilon \end{cases} \tag{17}$$

where $\boldsymbol{U}$ is the voltage matrix of the SRCPSS; $\boldsymbol{I}$ is the current matrix of the SRCPSS; λ_1-λ_n are the eigenvalues of the node admittance matrix $\boldsymbol{Y}$, which refers to the reciprocal of resonance impedance; $\boldsymbol{L}$ and $\boldsymbol{T}$ are the left and right eigenvector matrices, respectively; $\boldsymbol{\Lambda}$ is the eigenvalue matrix; V_n and J_n are the model voltage and current at the n^{th} node, respectively; and ε is the impedance setting value, which can be set according to the actual application conditions.

In the OG IV, the target price function is established as in (18) to ensure the minimum investment of LCL filter. The fitness value for OG IV is F_4.

$$F_4 = p_1(L_{1\text{-}k} + L_{2\text{-}k}) + p_2 C_k \tag{18}$$

where p_1 and p_2 are the price coefficients.

Four OGs are used in the optimization process, and the priority of the four OGs can be determined by setting the fitness values of F_1-F_3. The suppression of resonance is the most important OG, and OG III has the highest priority. If OG III is met, we set $F_3 = 0$; otherwise, $F_3 = a_3$. The purpose of OG I is to weaken the resonance caused by the excitation of HBs generated by the PQC. Therefore, OG I is the second important OG. If OG I is met, $F_1 = 0$; otherwise, $F_1 = a_1$. The stability of the control system is equally important; thus, a_2 can be set as a_1. If OG II is met, $F_2 = 0$; otherwise, $F_2 = a_2$. The total fitness value F_{Z} is obtained as:

$$\begin{cases} F_{\text{Z}} = F_1 + F_2 + F_3 + F_4 \\ a_3 > a_1 + a_2 > a_1 \ge a_2 >> F_4 \end{cases} \tag{19}$$

To avoid the adverse effect of the inertial weight on the optimization, the adaptive inertial weight is adopted, which is expressed as:

$$w^i(:,j) = \begin{cases} w_{\min} + \dfrac{(w_{\max} - w_{\min})(F_{\text{PB}} - F_{\text{PB,min}})}{F_{\text{PB,avg}} - F_{\text{PB,min}}} & F_{\text{PB}} \le F_{\text{PB,avg}} \\ w_{\max} & F_{\text{PB}} > F_{\text{PB,avg}} \end{cases} \tag{20}$$

where $w_{\min}$ and $w_{\max}$ are the minimum and maximum values of the inertial weight, respectively; F_{PB} is the individual optimal fitness value of the particle; $F_{\text{PB,min}}$ is the minimum individual optimal fitness value; and $F_{\text{PB,avg}}$ is the average individual optimal fitness value.

Finally, based on the improved particle swarm optimization algorithm, the multi-objective optimization design for the parameters in the PQC is determined, as shown in Fig. 7, where P_{B} is the individual optimal position; G_{B} is the global optimal position; and F_{GB} is the global optimal fitness value.

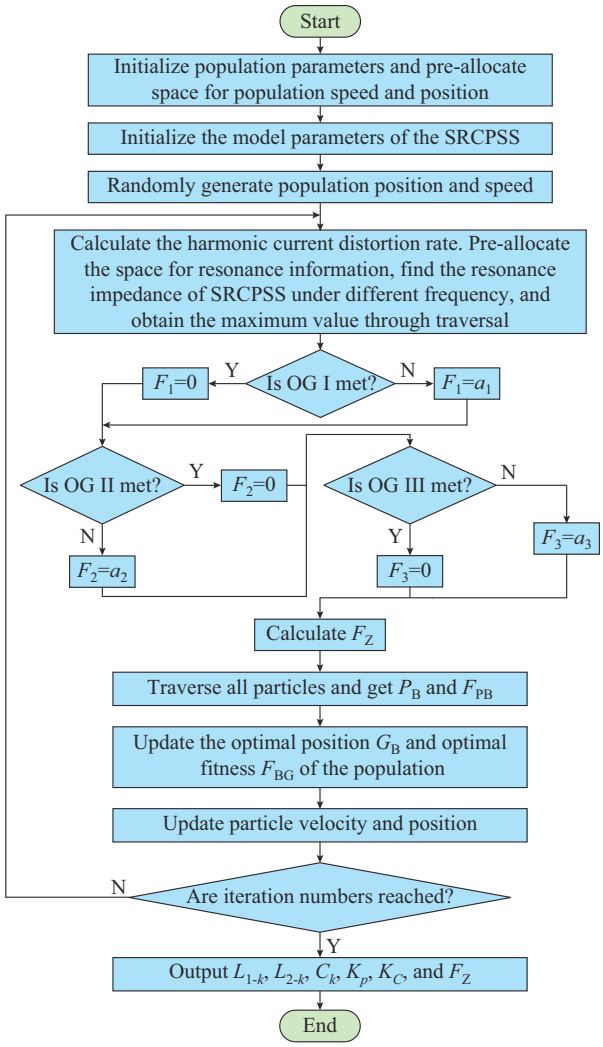

Fig. 7. Flow chart of multi-objective optimization design.

IV. Case Study Based on Field Test

The case study consists of three main parts. The first part obtains the possible current harmonics of the traction network in the SRCPSS through simulation and field test. The second part describes the resonance characteristics of the SRCPSS under different operating conditions. The third part deviates from the RBs of the HBs under the multi-objective optimization design. The actual suburban railways before and after renovation, as shown in Fig. 8, are analyzed to verify the effectiveness of the proposed design, and the parameters of this suburban railway line are listed in Table I, where S_{T1} and S_{ST} are the capacities of T1 and step-up transformer, respectively; and K_{T1}, K_{T2}, and K_{ST}

are the transformation ratios of T1, T2, and step-up transformer, respectively.

TABLE I
PARAMETERS OF A SUBURBAN RAILWAY LINE

Parameter	Value	Parameter	Value
S_{T1} (MVA)	40	K_C	5
S_{ST} (MVA)	6	L_1 (mH)	1
K_{T1}	4	L_2 (mH)	0.5
K_{T2}	11	C (μF)	20
K_{ST}	27.5	u_{dc} (V)	2200
K_p	4	u_{mk} (V)	1000
K_r	1000	f_{sw} (Hz)	3000

The basic information of the line is as follows. The line is part of a suburban railway in China and consists of three TSs and a section post (SP). Figure 8(a) shows the specific topology of the line before renovation. The traction transformers in the TS are connected in the form of a Vv shape. The SP is located among the three TSs, which enables the adjacent power supply sections to be connected in parallel or to operate independently. The state of the SP shows that the circuit breaker must be open because the system is powered in different phases. The three TSs can operate in continuous co-phase power supply mode after the PQC is put into operation and the lines are connected. The circuit breaker in the SP is closed, thereby enabling the power required by the electric locomotives to be provided jointly by the three TSs. Figure 3 illustrates the structure of a typical PQC, which consists of filters, a step-up transformer, and 12 back-to-back converters. The β- and α-phase converters are connected in cascade and parallel, respectively, through a multiwinding step-up transformer. The length of each traction network is shown in Fig. 8.

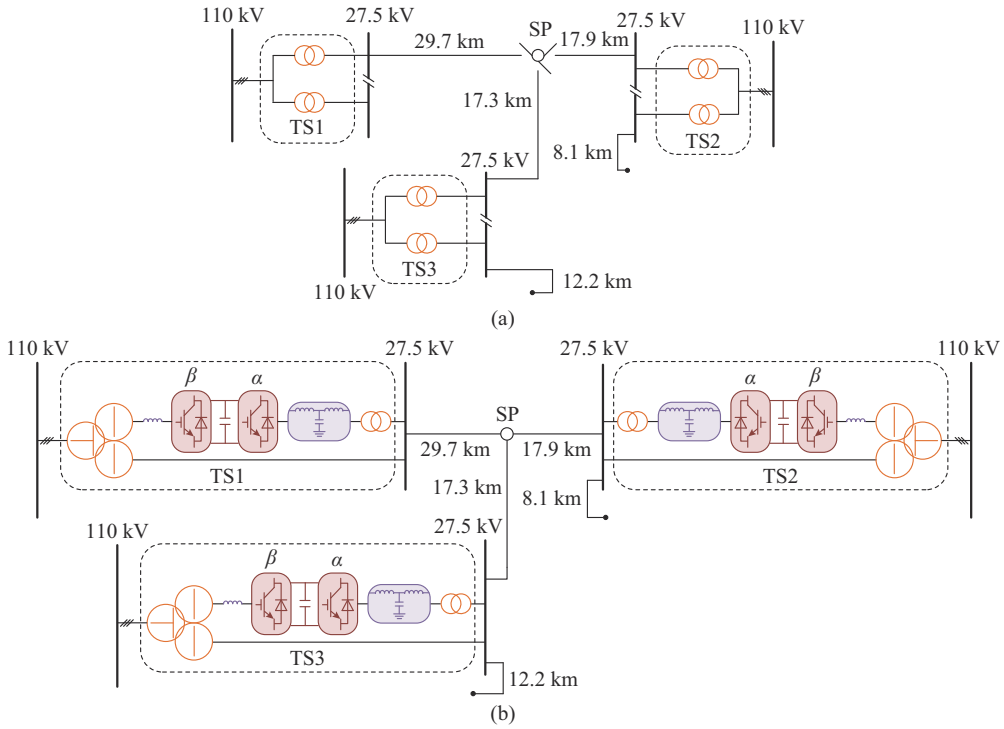

Fig. 8. Specific topologies of suburban railway line before and after renovation. (a) Before renovation. (b) After renovation.

The operation of each TS integrated with the PQC is tested before a continuous power supply is achieved (the circuit breaker in the SP remains open). Figure 9(a) shows a simplified test scenario, and Fig. 9(b) shows the specific processes of the field test and simulation. Each TS is equipped with a power quality remote monitoring device, which includes a power quality monitoring computer, a real-time power quality tester, and a communication device. The monitoring device measures the voltage and current of the feeder in the TS, and each synchronizes the sampling information of different measurement points using a global positioning system.

The operation of two locomotives is considered as a case to obtain the probability spectrum of the current harmonics in the traction network, as shown in Fig. 9(c). This is because the harmonics generated by the same type of locomotive and PQC in the steady state are nearly identical. Three relatively fixed current HBs (HB1-HB3) are clearly present in the traction network, where HB1 is generated by the PQC and locomotives, and HB2 and HB3 are mainly generated by the locomotives and PQC, respectively. The test and calculation results for each frequency band are consistent with the simulation results. A slight discrepancy is observed in the LF band, which may be attributed to the idealization of the converters in the simulation and the potential effects of factors such as the turn-on and turn-off impedances. Consequently, it is more efficacious to utilize the measured data for modeling purposes.

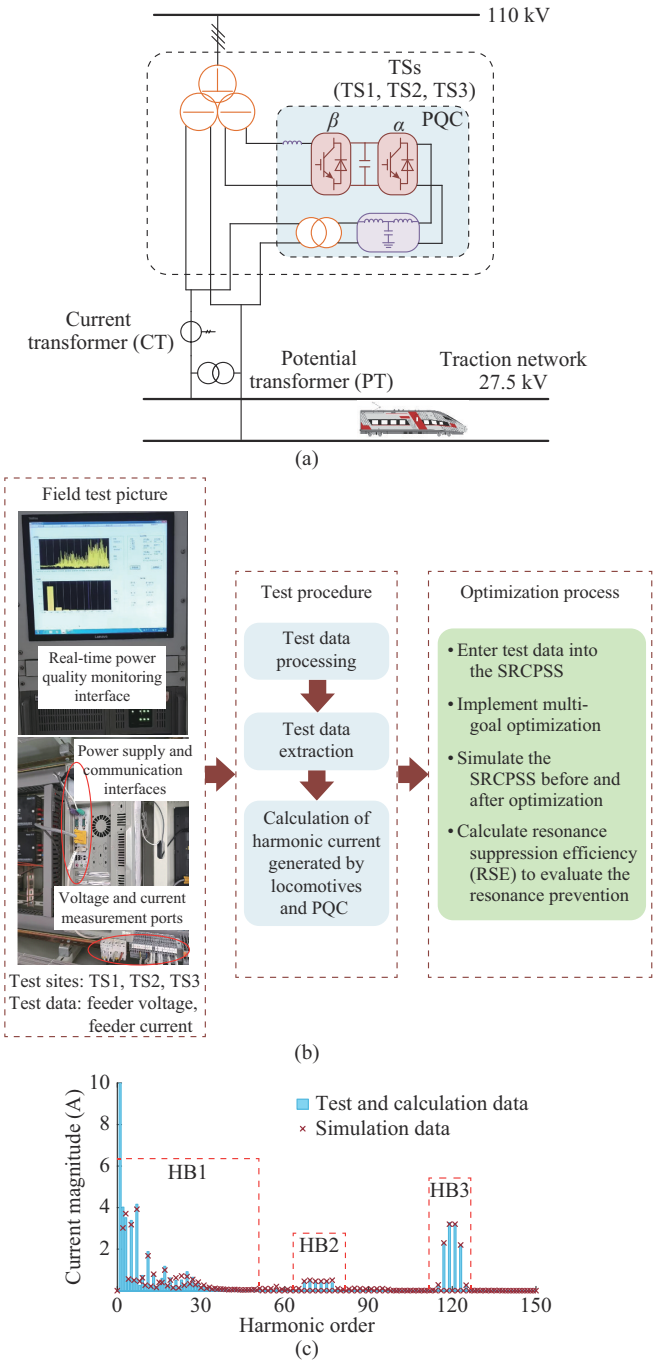

Fig. 9. Field test and simulation. (a) Simplified scenario diagram of field test. (b) Flow chart of case study based on field test. (c) Spectrum of harmonic current caused by PQC and electric locomotives.

Figure 10 shows the complete resonance characteristics of the SRCPSS under different operating conditions (the SRCPSS with three operating states of two, six, and ten locomotives are analyzed as cases, and the locomotives operate with low and high operating power in the SRCPSS). Three RBs are present in the SRCPSS with center harmonic orders (denoted by "X" in Fig. 10) of 32.6, 69.5, 76.1, and 122.7. The resonance below 50 harmonic orders is denoted as RB1, whereas that within 50-100 harmonic orders is denoted as RB2, and that exceeding 100 harmonic orders is denoted as RB3. The effects of different operating states on the resonance are summarized as follows.

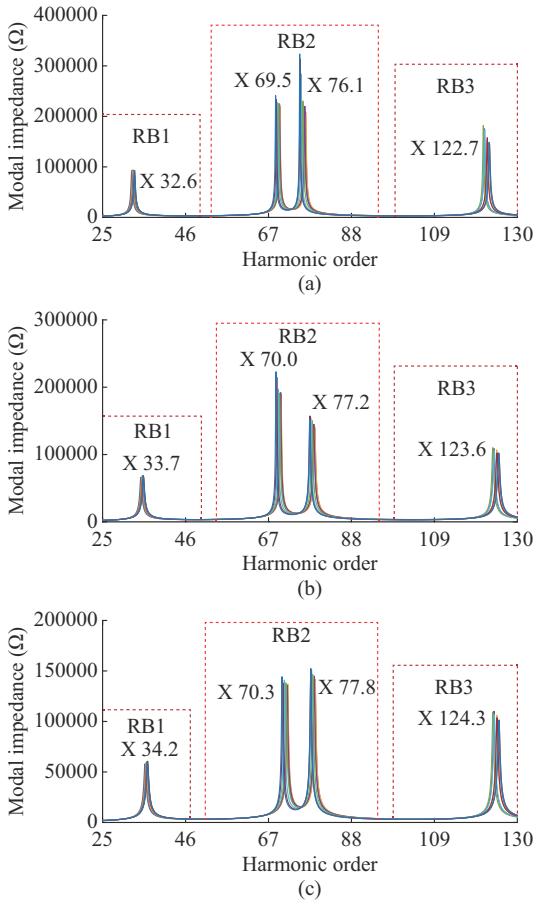

Fig. 10. Resonance distribution of SRCPSS under different operating conditions. (a) Two locomotives. (b) Six locomotives. (c) Ten locomotives.

1) The operating power of locomotive affects its equivalent resistance in the steady state. However, the resonance frequency remains relatively constant because the resonance is caused by the inductive and capacitive components of the SRCPSS.

2) As the locomotive moves, the resonance frequency and amplitude of the resonance impedance are no longer fixed. The resonance frequency fluctuates up to 30 Hz, whereas the resonance impedance exhibits a small range of variation.

3) The three RBs gradually shift to higher frequencies as the number of locomotives in the SRCPSS increases, but the variations in the RBs become less pronounced when the number of locomotives exceeds six. Therefore, in contrast to the "resonance point" in the conventional research works, special attention must be paid to the RBs with harmonic orders of 32.6-34.2, 69.2-70.3, 76.1-78.0, and 122.7-124.3 when the SRCPSS is in operation.

The resonance law is summarized as follows.

1) K_p, K_C, L_1, L_2, and C all have different degrees of influence on the frequencies and amplitudes of RB1 and RB2, whereas K_i practically has no effect on the resonance, which is consistent with the analysis presented in Section II.

2) Changes in K_p, K_C, L_1, L_2, and C result in a sharp reduction in the resonance peaks, as shown in Supplementary Material B Fig. B1 region A, indicating that the PQC can be designed to significantly reduce the harmonic voltage of the SRCPSS.

3) Changes in the aforementioned parameters lead to abrupt changes in resonance frequencies, as shown in Supplementary Material B Fig. B1 regions 1, 2, and 3. For example, the frequency of region 1 gradually decreases with an increase in the parameters, but region 1 mutates into region 2 with further expansion of the given parameters. Resonance can also be suppressed by shifting the resonance frequency, thereby reducing its coincidence with the harmonic frequency, which is consistent with the effects of reducing the resonance peaks.

In summary, changes in the parameters may cause the occurrence of new RBs and the attenuation of some RBs. Therefore, the effects of the parameters on resonance must be comprehensively considered, and prevention of resonance must be realized through optimization.

The range of the control parameters is then set according to the constraints. Five poles are present in the control system, and most of the real parts of poles 1, 4, and 5 are less than 0. Therefore, only the changes in the real parts of poles 2 and 3 are shown in Fig. 11. The blank parts are poles whose real parts are larger than 0, and the colored parts are the poles whose real parts are smaller than 0. Based on the distributions of poles 2 and 3, area A is selected as the acceptable range for K_p and K_C.

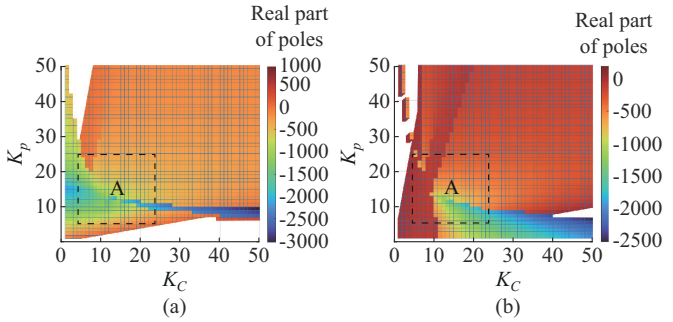

Fig. 11. Pole distribution of control system when K_C and K_p change. (a) Pole 2. (b) Pole 3.

Figure 12 shows that the total fitness value and resonance distribution of the optimized SRCPSS are output consecutively once the algorithm reaches the maximum number of iterations. The particles fluctuate in searching for the optimal solution, and the total fitness value F_Z stabilizes and reaches the lowest value after 150 iterations ($F_Z = F_4 = 0.76 \times 10^{-3}$, and F_1, F_2, and F_3 are all 0). At this time, the control parameters K_p and K_C are 7.75 and 7.87, respectively, L_1 is 0.78 mH, L_2 is 0.15 mH, and C is 57.9 μF. As Fig. 12(b) shows, the resonance impedance in the harmonic frequency band is completely reshaped to avoid resonance accidents when the proposed method is adopted by the PQC. The HBs and RBs do not coincide under either the light-load mode with two locomotives or the heavy-load mode with ten locomotives, which satisfies the OG III.

As Fig. 13 shows, the operation of the optimized PQC is first verified under multi-locomotive operating conditions without resonance. The HF harmonic current distortion rate of the PQC is less than 0.3% under both the light-load and heavy-load conditions, which proves that the proposed design can assist the PQC in meeting the OG I.

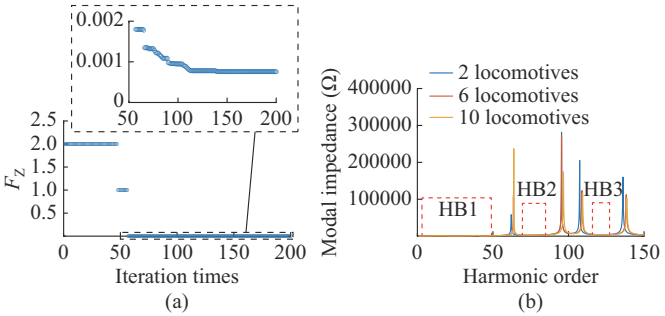

Fig. 12. Iteration process and resonance distribution of SRCPSS after optimization. (a) Iteration process. (b) Resonance distribution.

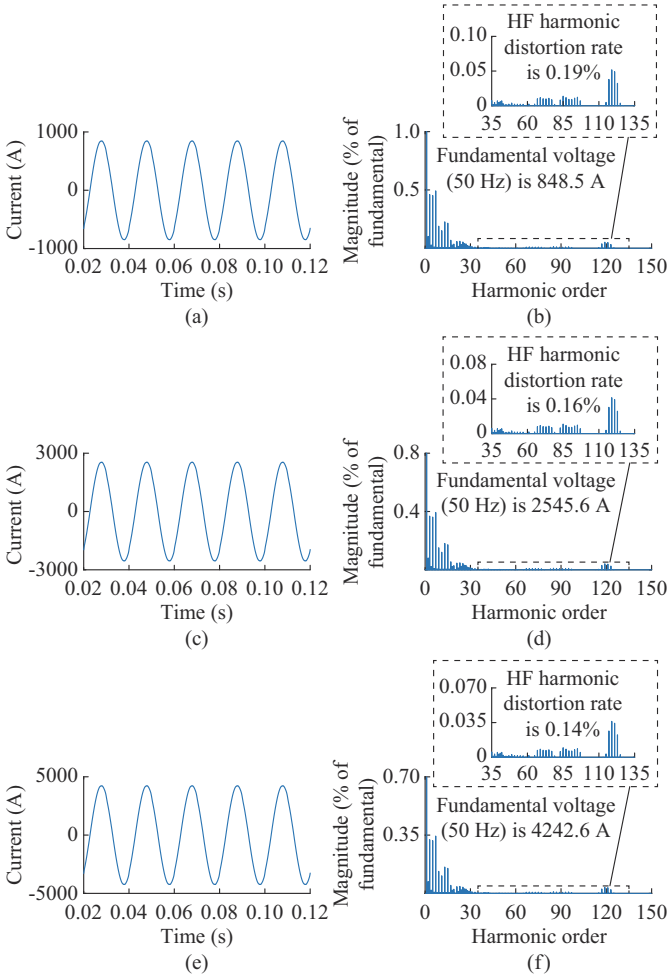

Fig. 13. Operation of PQC under multi-locomotive operating conditions without resonance using proposed method. (a) Current i_k with two locomotives. (b) Fast Fourier transform (FFT) result of i_k with two locomotives. (c) Current i_k with six locomotives. (d) FFT result of i_k with six locomotives. (e) Current i_k with ten locomotives. (f) FFT result of i_k with ten locomotives.

The resonance occurring in the SRCPSS is further simulated based on the actual model data for each component. The resonance in the SRCPSS under multi-locomotive operating conditions is observed, as shown in Fig. 14. The resonance is most severe when two locomotives are running. The voltage of the traction network exceeds 49 kV, causing the SRCPSS to trip momentarily. The FFT analytical results show that RB2 and RB3 of the SRCPSS are excited by HB2

and HB3, respectively, and the distortion rate reaches 26.98%, which is much higher than 5% specified in IEEE Standard 519-2022. In addition, based on the field test data, the resonance is simulated for operations with six and ten locomotives. When the number of locomotives gradually increases, the RB gradually moves to a high frequency, resulting in a gradual decrease in the overlapping areas of HB1, HB2, and HB3 with RB1, RB2, and RB3, respectively. Therefore, the harmonic voltage distortion rate is reduced from 26.98% to 8.33%, which is consistent with the results shown in Fig. 10.

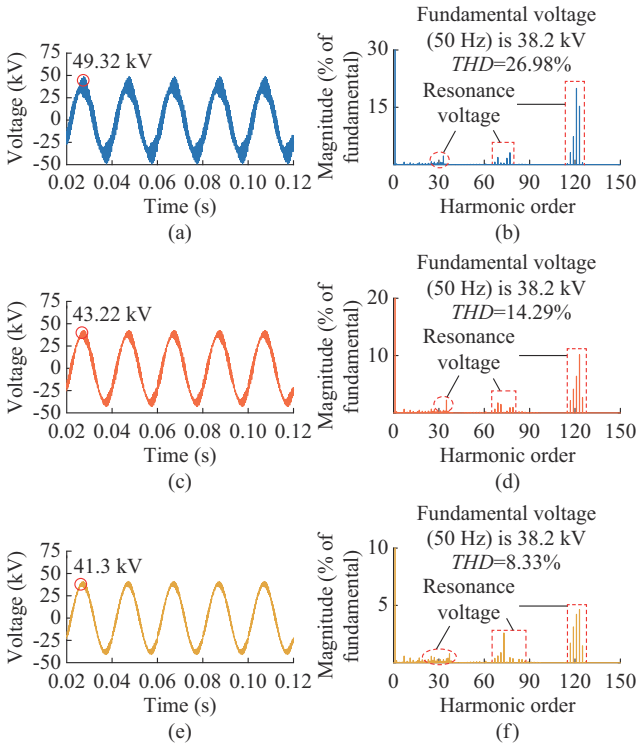

Fig. 14. Voltage waveform and spectrum of traction network based on test data before using proposed method. (a) Voltage waveform with two locomotives. (b) Spectrum with two locomotives. (c) Voltage waveform with six locomotives. (d) Spectrum with six locomotives. (e) Voltage waveform with ten locomotives. (f) Spectrum with ten locomotives.

To verify the accuracy of theoretical analysis and demonstrate the reasonableness of the test data, the voltage waveforms and spectra of the traction network simulated using MATLAB/Simulink are recorded, as shown in Fig. 15. The distribution of harmonics in the frequency band is nearly identical to the results shown in Fig. 14. An analysis on Fig. 9 reveals that a discrepancy exists between the simulation and test data at LFs, and thus the LF harmonics are lower than the results presented in Fig. 14. However, resonance typically occurs at HFs. Therefore, the LF discrepancy does not affect the resonance in this paper. In addition, as the number of locomotives increases, the change rule of the resonance voltage aligns with that shown in Fig. 14, which again verifies the correctness of theoretical analysis.

Finally, the optimized PQC is connected to the SRCPSS in the resonance case. The voltage of the traction network is measured under the operating conditions with two, six, and ten locomotives, and the voltage waveforms and spectra of the traction network are obtained, as shown in Fig. 16. The voltage waveform is sufficiently smooth, with the peak value maintained at approximately 38.2 kV both in the light-load mode with two locomotives and heavy-load mode with ten locomotives. This demonstrates that the resonance overvoltage problem is suppressed by the proposed method. FFT analytical results show that the intrinsic resonance of the SRCPSS is not excited by HB1, HB2, or HB3. The distortion rates are 1.28%, 1.12%, and 0.82%, respectively, which are all less than 5%, and the individual harmonic distortion rate is less than 3%, which is consistent with the results shown in Fig. 12.

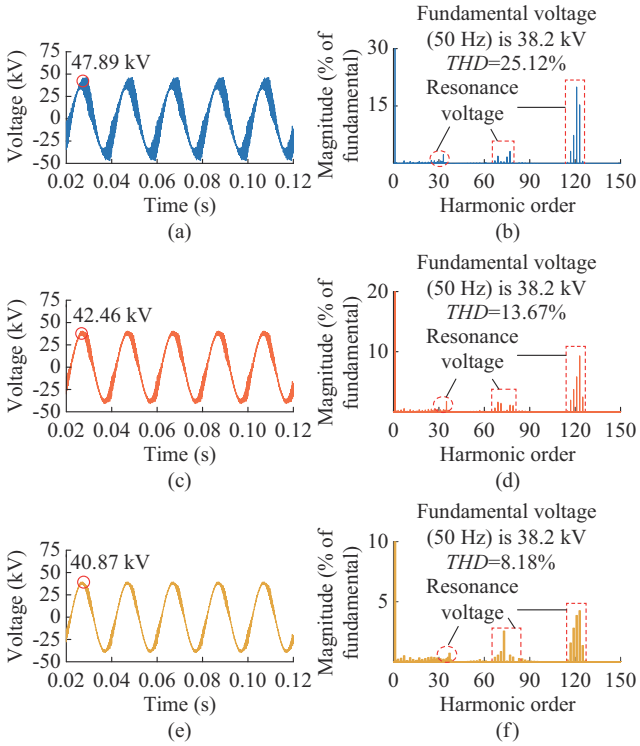

Fig. 15. Voltage waveform and spectrum of traction network based on simulation data before using proposed method. (a) Voltage waveform with two locomotives. (b) Spectrum with two locomotives. (c) Voltage waveform with six locomotives. (d) Spectrum with six locomotives. (e) Voltage waveform with ten locomotives. (f) Spectrum with ten locomotives.

Previous analysis demonstrates that the wideband harmonics generated by power electronic equipment such as PQCs and electric locomotives have the potential to stimulate the RBs present in the SRCPSS. Consequently, it is essential to consider both harmonic and resonance issues as well as the control effect of the PQC prior to connecting it to the TS.

Based on the voltage data of the traction network obtained from Figs. 14 and 16, the RSE is calculated to evaluate the proposed method, as given in (21). The harmonics in the voltage harmonic spectrum that significantly affect the total harmonic distortion rate are referred to as dominant harmonics. Therefore, with the operation of two locomotives with the most severe resonance used as a case, the RSE of the dominant harmonics is calculated, as shown in Table II.

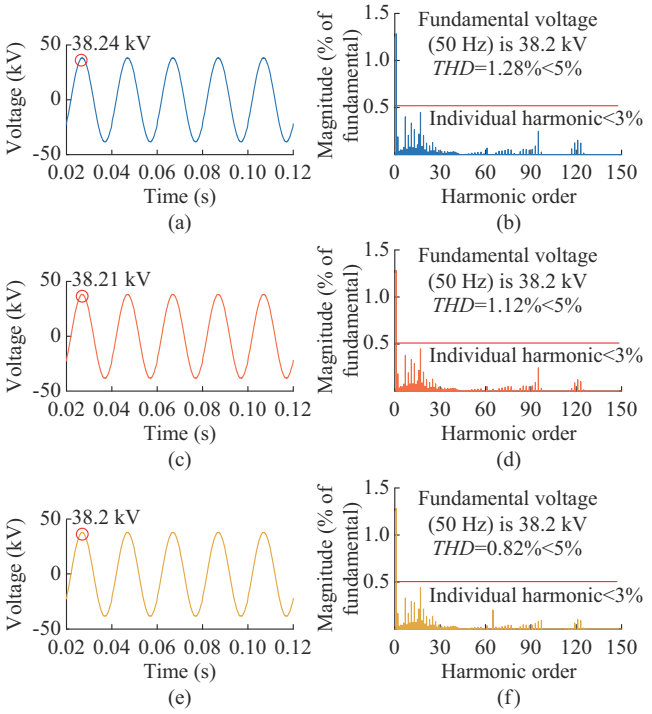

Fig. 16. Voltage waveform and spectrum of traction network based on test data after using proposed method. (a) Voltage waveform with two locomotives. (b) Spectrum with two locomotives. (c) Voltage waveform with six locomotives. (d) Spectrum with six locomotives. (e) Voltage waveform with ten locomotives. (f) Spectrum with ten locomotives.

TABLE II
RSE OF DOMINANT HARMONICS

Harmonic order	RSE (%)	Harmonic order	RSE (%)
25	81.18	75	96.42
27	87.07	77	98.26
31	94.57	79	93.65
32	96.72	115	98.86
33	98.43	117	97.85
67	97.03	119	98.10
69	97.88	121	99.15
71	90.91	123	99.11
73	87.86	125	96.61

$$\gamma_h = \frac{ru_{h,\text{before}} \cdot u_{1,\text{before}} - ru_{h,\text{after}} \cdot u_{1,\text{after}}}{ru_{h,\text{before}} \cdot u_{1,\text{before}}} \times 100\% \qquad (21)$$

where $ru_{h,\text{before}}$ and $ru_{h,\text{after}}$ are the rates of the h^{th} harmonic content before and after applying the proposed method, respectively; and $u_{1,\text{before}}$ and $u_{1,\text{after}}$ are the amplitudes of the fundamental voltage before and after applying the proposed method, respectively.

The resonance orders are 31-33, 67-71, 77-79, and 117-123. Table II shows that the suppression efficiency of the proposed method for the resonance voltage exceeds 90%, which fully controls the resonance to ensure the safe operation of SRCPSS.

V. CONCLUSION

In this paper, an analytical method and field test are combined to establish a model of SRCPSS, and a modal scanning algorithm suitable for resonance analysis of SRCPSS is then used to explore the effects of the parameters of the PQC on the resonance. Based on the resonance characteristics, a multi-objective optimization design for the PQC is then proposed to solve a series of problems caused by resonance. Finally, a simulation based on a field test is used to verify the effectiveness of the proposed method. The findings are summarized as follows.

1) The complete resonance characteristics of the SRCPSS obtained by the modal scanning algorithm show that the wide-band resonance appears in SRCPSS due to the movement of electric locomotives, the number of locomotives, and the addition of the PQC.

2) Changes in L_1, L_2, C, K_p, and K_C in the PQC lead to large and irregular changes in the resonance frequency and impedance amplitude, which may exacerbate the resonance. A reasonable setting of these parameters can realize remodeling of the impedance characteristics.

3) Based on the changes in resonance characteristics derived from the PQC, a multi-objective optimization design for the PQC is proposed with the objective of resonance suppression, stability maintenance, harmonic filtering and cost reduction. The results reveal that the suppression efficiency of the proposed method for the resonance voltage exceeds 90%, indicating that resonance does not occur under different operating conditions.

REFERENCES

[1] Q. Li, "On new generation traction power supply system and its key technologies for electrification railway," *Journal of Southwest Jiaotong University*, vol. 49, no. 4, pp. 559-568, Jun. 2014.
[2] Z. Cai, T. Li, X. Su *et al.*, "Research on analysis method of characteristics generation of urban rail transit," *IEEE Transactions on Intelligent Transportation Systems*, vol. 21, no. 9, pp. 3608-3620, Sept. 2020.
[3] J. Yang, X. Lin, H. Zhu *et al.*, "FPGA-based digital implementation of flexible power control for three-phase to single-phase MMC-based advanced co-phase traction power supply system," *Journal of Modern Power Systems and Clean Energy*, vol. 11, no. 6, pp. 2015-2027, Nov. 2023.
[4] L. Liu, N. Dai, K. Lao *et al.*, "A co-phase traction power supply system based on asymmetric three-leg hybrid power quality conditioner," *IEEE Transactions on Vehicular Technology*, vol. 69, no. 12, pp. 14645-14656, Dec. 2020.
[5] L. Zhang, S. Liang, X. Li *et al.*, "Modelling on novel cable traction power supply system and power distribution analysis," *IEEE Transactions on Power Delivery*, vol. 37, no. 2, pp. 745-754, Apr. 2022.
[6] F. Ma, Q. Xu, Z. He *et al.*, "A railway traction power conditioner using modular multilevel converter and its control strategy for high-speed railway system," *IEEE Transactions on Transportation Electrification*, vol. 2, no. 1, pp. 96-109, Mar. 2016.
[7] C. Zhao, Q. Jiang, and D. Liu, "Flexible power supply system of AC electric arc furnace," *Journal of Modern Power Systems and Clean Energy*, vol. 11, no. 2, pp. 622-633, Mar. 2023.
[8] Q. Xu, F. Ma, Z. He *et al.*, "Analysis and comparison of modular railway power conditioner for high-speed railway traction system," *IEEE Transactions on Power Electronics*, vol. 32, no. 8, pp. 6031-6048, Aug. 2017.
[9] Z. Shu, S. Xie, K. Lu *et al.*, "Digital detection, control, and distribution system for co-phase traction power supply application," *IEEE Transactions on Industrial Electronics*, vol. 60, no. 5, pp. 1831-1839, May 2013.
[10] W. Song, S. Jiao, Y. Li *et al.*, "High-frequency harmonic resonance suppression in high-speed railway through single-phase traction con-

verter with LCL filter," *IEEE Transactions on Transportation Electrification*, vol. 2, no. 3, pp. 347-356, Sept. 2016.
[11] F. Zhong and S. Xie, "Study on resonance characteristic of continuous co-phase traction power supply system," *IET Generation, Transmission & Distribution*, vol. 17, no. 4, pp. 775-789, Dec. 2022.
[12] Y. Zhao, L. Ren, G. Lin *et al*., "Research on the harmonics penetration characteristics of the traction network to three-phase 380 V power system of the traction substation and suppression scheme," *IEEE Access*, vol. 8, pp. 195359-195369, Oct. 2020.
[13] H. Hu, S. Gao, Y. Shao *et al*., "Harmonic resonance evaluation for hub traction substation consisting of multiple high-speed railways," *IEEE Transactions on Power Delivery*, vol. 32, no. 2, pp. 910-920, Apr. 2017.
[14] H. Lee, C. Lee, G. Jang *et al*., "Harmonic analysis of the Korean high-speed railway using the eight-port representation model," *IEEE Transactions on Power Delivery*, vol. 21, no. 2, pp. 979-986, Apr. 2006.
[15] L. Sainz, M. Caro, and E. Caro, "Analytical study of the series resonance in power systems with the Steinmetz circuit," *IEEE Transactions on Power Delivery*, vol. 24, no. 4, pp. 2090-2098, Oct. 2009.
[16] X. Wu, S. Sadullah, B. Matthews *et al*., "Nodal harmonic impedance derivation of AC network in PSS/E," in *Proceedings of 9th IET International Conference on AC and DC Power Transmission (ACDC 2010)*, London, UK, Oct. 2010, pp. 1-5.
[17] Z. He, H. Hu, Y. Zhang *et al*., "Harmonic resonance assessment to traction power-supply system considering train model in China high-speed railway," *IEEE Transactions on Power Delivery*, vol. 29, no. 4, pp. 1735-1743, Aug. 2014.
[18] K. Song, M. Wu, S. Yang, *et al*., "High-order harmonic resonances in traction power supplies: a review based on railway operational data, measurements, and experience," *IEEE Transactions on Power Electronics*, vol. 35, no. 3, pp. 2501-2518, Mar. 2020.
[19] W. Xu, Z. Huang, Y. Cui *et al*., "Harmonic resonance mode analysis," *IEEE Transactions on Power Delivery*, vol. 20, no. 2, pp. 1182-1190, Apr. 2005.
[20] Y. Cui and X. Wang, "Modal frequency sensitivity for power system harmonic resonance analysis," *IEEE Transactions on Power Delivery*, vol. 27, no. 2, pp. 1010-1017, Apr. 2012.
[21] L. Hong, W. Shu, J. Wang *et al*., "Harmonic resonance investigation of a multi-inverter grid-connected system using resonance modal analysis," *IEEE Transactions on Power Delivery*, vol. 34, no. 1, pp. 63-72, Feb. 2019.
[22] K. Song, G. Konstantinou, M. Wu *et al*., "Windowed SHE-PWM of interleaved four-quadrant converters for resonance suppression in traction power supply systems," *IEEE Transactions on Power Electronics*, vol. 32, no. 10, pp. 7870-7881, Oct. 2017.
[23] L. Wu and M. Wu, "Single-phase cascaded *H*-bridge multi-level active power filter based on direct current control in AC electric railway application," *IET Power Electronics*, vol. 10, no. 6, pp. 637-645, May 2017.
[24] H. Hu, Z. He, and S. Gao, "Passive filter design for China high-speed railway with considering harmonic resonance and characteristic harmonics," *IEEE Transactions on Power Delivery*, vol. 30, no. 1, pp. 505-514, Feb. 2015.
[25] A. Luo, Q. Xu, F. Ma *et al*., "Overview of power quality analysis and control technology for the smart grid," *Journal of Modern Power Systems and Clean Energy*, vol. 4, no. 1, pp. 1-9, Jan. 2016.
[26] P. S. A. Peiris, S. Filizadeh, and D. Muthumuni, "Improved state-space modelling for microgrids without virtual resistances," *Journal of Modern Power Systems and Clean Energy*, vol. 12, no. 2, pp. 584-596, Mar. 2024.
[27] S. K. Panda and B. Subudhi, "A review on robust and adaptive control schemes for microgrid," *Journal of Modern Power Systems and Clean Energy*, vol. 11, no. 4, pp. 1027-1040, Jul. 2023.
[28] Y. Wang, X. Zhou, J. Tang *et al*., "Adaptive harmonic virtual impedance control for improving voltage quality of microgrids," *Journal of Modern Power Systems and Clean Energy*, vol. 12, no. 5, pp. 1548-1558, Sept. 2024.
[29] Z. Shuai, H. Cheng, J. Xu *et al*., "A notch filter-based active damping control method for low-frequency oscillation suppression in train-network interaction systems," *IEEE Journal of Emerging and Selected Topics in Power Electronics*, vol. 7, no. 4, pp. 2417-2427, Jan. 2019.
[30] H. Safamehr, T. Najafabadi, and F. Salmasi, "Adaptive control of grid-connected inverters with nonlinear LC filters," *IEEE Transactions on Power Electronics*, vol. 38, no. 2, pp. 1562-1570, Feb. 2023.
[31] S. Jayalath and M. Hanif, "Generalized LCL-filter design algorithm for grid-connected voltage-source inverter," *IEEE Transactions on Industrial Electronics*, vol, 64, no. 3, pp. 1905-1915, Mar. 2017.
[32] C. Poongothai and K. Vasudevan, "Design of LCL filter for grid-interfaced PV system based on cost minimization," *IEEE Transactions on Industry Applications*, vol. 55, no, 1, pp. 584-592, Jan.-Feb. 2019.
[33] Y. Cai, Y. He, H. Zhou *et al*., "Design method of LCL filter for grid-connected inverter based on particle swarm optimization and screening method," *IEEE Transactions on Power Electronics*, vol. 36, no. 9, pp. 10097-10113, Sept. 2021.
[34] P. Chen, W. Zhao, X. Chen *et al*., "An impedance-based parameter design method for active damping of load converter station in MTDC distribution system," *Journal of Modern Power Systems and Clean Energy*, vol. 10, no. 5, pp. 1423-1436, Sept. 2022.
[35] J. Qi, Q. Wu, Y. Zhang *et al*., "Unified residue method for design of compact wide-area damping controller based on power system stabilizer," *Journal of Modern Power Systems and Clean Energy*, vol. 8, no. 2, pp. 367-376, Mar. 2020.
[36] X. Wu, Y. Xu, X. Wu *et al*., "A two-layer distributed cooperative control method for islanded networked microgrid systems," *IEEE Transactions on Smart Grid*, vol. 11, no. 2, pp. 942-957, Mar. 2020.
[37] Q. Liu, F. Liu, R. Zou *et al*., "Harmonic resonance characteristic of large-scale PV plant: modelling, analysis, and engineering case," *IEEE Transactions on Power Delivery*, vol. 37, no. 3, pp. 2359-2368, Jun. 2022.
[38] H. Cui, X. Feng, J. Zhang *et al*., "Harmonic characteristic analysis of carrier based pulse-width modulation traction rectifier," *Transactions of China Electrotechnical Society*, vol. 28, no. 9, pp. 21-31. Sept. 2013.

Fan Zhong received the B.S. degree in electrical engineering from Xihua University, Chengdu, China, in 2020, and the M.S. degree in electrical engineering from Southwest Jiaotong University, Chengdu, China, in 2023. He is currently pursuing the Ph.D. degree with the School of Electrical Engineering, Southwest Jiaotong University, Chengdu, China. His research interests include traction power supply system, harmonic resonance, and stability analysis.

Shaofeng Xie received the B.S., M.S., and Ph.D. degrees in electrical engineering from Southwest Jiaotong University, Chengdu, China, in 1998, 2001, and 2004, respectively. Since 2013, he has been a Professor with the School of Electrical Engineering, Southwest Jiaotong University. He is currently the Vice Dean of the School of Electrical Engineering. His research interests include traction power system analysis, power quality, and power electronics.

You Peng received the B.S. degree in mineral processing engineering from Panzhihua University, Panzhihua, China, in 2018. He is currently pursuing the Ph.D. degree with the School of Electrical Engineering, Southwest Jiaotong University, Chengdu, China. His research interests include traction power system analysis, power quality, energy system, and power electronics.

Xinyao Hu received the B.S. degree in electrical engineering from Southwest Jiaotong University, Chengdu, China, in 2022. He is currently pursuing the M.S. degree in the School of Electrical Engineering, Southwest Jiaotong University, Chengdu, China. His research interests include traction power supply system and harmonic resonance.